

EXPERIMENTAL INVESTIGATION OF FLOWFIELD OVER A MULTI-ELEMENT AEROFOIL AND COMPARISON WITH COMPUTATIONAL PREDICTION

S.R. Maddah, Dr H.H. Bruun

Department of Mechanical and Medical Engineering, Fluid Flow Division, University of Bradford, Bradford, BD7 1DP

Keywords: *Multi-element aerofoil, FHW, RSM*

Abstract

This paper presents results obtained from a combined experimental and computational study of the flowfield over a multi-element aerofoil with and without an advanced slat. Detailed measurement of the mean flow and turbulent quantities over a multi-element aerofoil model in a wind tunnel have been made using pressure, stationary and flying hot-wire (FHW) probes. The model configuration spans the test section and is made of three parts: 1) an advanced slat, 2) a NACA 4412 main aerofoil, 3) a NACA 4415 flap. The chord lengths of the elements were 38, 250 and 83 mm respectively. The results were obtained at a chord Reynolds number of 2.5×10^5 and a free Mach number of less than 0.1. The slat performance at different angles of attack, α , were investigated and compared with cases without the slat. Numerical predictions have been obtained by solving the time-averaged Navier-Stokes equations incorporating a Reynolds Stress Model (RSM) for the same configurations. This paper presents results for both experimental and numerical selected cases placing the multi-element aerofoil at angles of attack of 15° and 20° with the advanced slat and 5° and 15° without employing the advanced slat. The computational results are compared with experimental data, which showed excellent agreement for low angle of attack and good agreement for other cases without separation, taking into account errors in both the experimental and numerical results. However, discrepancies were in particular observed in the

complicated shear layers and high turbulent intensity regions due to limitations in the turbulence model and also inadequate grid resolution.

1 Introduction

High-lift systems are used on aircrafts to provide adequate low speed performance in terms of approach speed and take-off and landing field lengths. Leading-edge devices such as slats and Kruger flap are commonly used to delay stall to higher angles of attack and consequently increase the maximum lift performance, C_{Lmax} . Studies are available which present data on slatted and flapped configurations. Conventional slat performance in high lift systems was studied by a number of researchers [1-4]. Since slat cove separation is minimised for the advanced slat due to its smooth and heel-less lower surface, it produces less drag compared to a conventional slat with lower surface discontinuity [5]. Laser Doppler Velocimeters (LDV) have been used to measure mean and fluctuating velocities around three-element aerofoils [1]. Several researchers have measured other related quantities such as C_p , C_L and C_M [6,7]. One of the previous experimental works is of particular importance since it deals with measurement of velocity and turbulent quantities at two angles of attack, $\alpha = 10^\circ$ and $\alpha = 18^\circ$ [8]. Further experiments of mean velocity and turbulence quantities in the slat and flap cove regions have been undertaken [9,10]. The former reported pressure distributions for a range of 0° to 20° and the latter presented

mainly velocity distributions in the slat and flap cove regions at angles of attack of 10° and 14° .

Methods for computing flows around high-lift systems of multi-element aerofoils are still providing major challenging problems. The presence of confluent boundary layers, wakes and turbulent boundary layer separation remain substantial challenges for accurate and efficient computation of lift and drag for different multi-element aerofoil configurations. Several computational methods for solving the Navier-Stokes equations for multi-element aerofoil flows have been reported [8-16]. Since a single structured grid can not be generated around a multi-element aerofoil, unstructured [10] and multiple structured grids [8-9] are usually used. For complex turbulent flows, the choice of the turbulence model can have a large impact on the accuracy of the results and computational expense. Simple algebraic models, such as the Baldwin-Lomax model, have been used extensively and successfully for single aerofoil models, especially for the case of attached flow [11]. The $k-\varepsilon$ turbulence model, one of the most widely used and validated turbulence models, has been used for a number of multi-element aerofoil computational investigations [12-14]. The most complex classical turbulence model is the Reynolds stress model which solves the differential transport equations for the Reynolds stresses (DSM) or solves the differential transport equations for the Reynolds stresses and Reynolds fluxes (DFM). Several major drawbacks of the $k-\varepsilon$ model emerge when the RSM model is used to predict flows with complex strain fields (e.g. curved boundary layers, swirling flows). Consequently a number of researchers have used the RSM model to predict flowfields around multi-element aerofoils [15-16].

The present research is an investigation of the flowfields over the multi-element aerofoil using mainly flying hot-wire X probes to highlight flow field improvement due to slat performance at different angles of attack (i.e. 5° , 10° , 15° , 17.5° , 20° , 22.5° and 25°) for both deflected and non-deflected flap. The acquired data were analysed and \overline{U} , \overline{V} , $\overline{u^2}$, $\overline{v^2}$, \overline{uv} were

calculated in each case. This paper first presents detailed measurements of the mean velocity of the turbulent flow in the vicinity of a two-element aerofoil for angles of attack of 5° and 15° and results for the multi-element aerofoil at angles of attack of 15° and 20° with the advanced slat. This is followed by numerical predictions of the mean velocity for the same configurations. Finally the experimental observations are compared with the computational results.

2 Experimental Arrangement and Test Conditions

The experiments were conducted in a low speed wind tunnel of University of Bradford having a 600×600 mm cross section. The model configuration spans the test section and it is made of three parts: 1) an advanced slat, 2) a NACA 4412 main aerofoil, 3) a NACA 4415 flap. The chord lengths of the elements were 38, 250 and 83 mm respectively. The free stream velocity was set at 18m/s and the corresponding Reynolds number based on main aerofoil chord length was 2.5×10^5 .

Two-dimensionality was validated after making the following observations: Measurement of the mean velocity profile at different spanwise location and comparison of them showed negligible variation about the centreline profile with and without the slat for 90% of span width.

The main experimental technique of present research was a flying hot-wire mounted on a precise computer-controlled mechanism. The rectification problem which is common for stationary hot-wire probes when measuring reversed flow was thus avoided by biasing the relative velocity. The basic principle of the FHW can be explained with reference to figure 1. Consider a surface with a (two-dimensional) separated flow region. A space-fixed coordinate system is introduced, in which the flow velocity vector \vec{V} and its velocity components U and V are to be calculated. Based on the geometry of the flying hot-wire mechanism, the probe sensors will follow a prescribed curve (a).

At time t , the probe is assumed to be at a known position (x_p, y_p) and move with a known velocity \vec{V}_p . The moving hot-wire probe is exposed to the relative velocity \vec{V}_r , and this velocity vector for a X probe is normally evaluated in terms of the velocity components $[U_r', V_r']$ in a probe-stem aligned co-ordinate system. Provided the orientation of the probe stem relative to the space-fixed coordinate system is known, then the corresponding space-fixed velocity components $[U_r, V_r]$ can be calculated. Having measured \vec{V}_p and \vec{V}_r the flow vector \vec{V} is obtained from

$$\vec{V} = \vec{V}_r + \vec{V}_p \quad (1)$$

as illustrated in figure 1. Provided that the magnitude of the probe velocity $|\vec{V}_p|$ is greater than the magnitude of the flow velocity $|\vec{V}|$, the relative velocity vector \vec{V}_r will remain within the approach quadrant of the X probe and the hot-wire signals can be interpreted uniquely [17].

The principle of the mechanical implementation for the bean shaped curve path used at Bradford University is illustrated in figure 2. Details of Bradford University's flying hot-wire system is given in [18-19].

3 Measurement Procedure and Results

Measurements were obtained from a number of points on the lower part of the probe curve path on figure 2 during a single sweep, and for this experimental study, 20 evenly spaced points were selected for detailed analysis. The sweep was repeated N times and ensemble average was used to calculate the mean velocity components, \overline{U} and \overline{V} , and the turbulent quantities, $\overline{u^2}$, $\overline{v^2}$ and \overline{uv} .

3.1 Main aerofoil at $\alpha=5^\circ$ and flap at $\delta_f=0^\circ$

Figure 3 shows the mean velocity vectors results for the main aerofoil at an angle of attack of $\alpha = 5^\circ$ equipped with a non-deflected flap. The velocity vectors indicate that the flow is attached to the model surface and there is no sign of separation. An accelerated flow over the

leading edge of main aerofoil is responsible for creating suction and lift. The maximum velocity in this region reaches a peak value of ($\sim 1.3 U_\infty$). The asymmetric wake is narrow and the velocity deficit is small over the trailing edge of the main aerofoil and the flap. The flow is seen to have recovered one chord length beyond the trailing edge of the flap. The minimum velocities of about 10 m/s are observed over the trailing edge of main aerofoil. This flowfield pattern is similar to the one reported in [15].

3.2 Main aerofoil at $\alpha=15^\circ$ and flap at $\delta_f=0^\circ$

The mean velocity vectors for the NACA 4412 main aerofoil at an angle of attack $\alpha=15^\circ$ and with a flap deflection angle of 0° are shown in figure 4. The experimental data for the flow over the two-element aerofoil clearly shows that a large region of recirculating flow exists over the main aerofoil. This deterioration in the flow field causes considerable loss of lift. The large velocity deficit is seen to persist further downstream, beyond a distance of one chord length from the trailing-edge of the main aerofoil. The flap gap flow is observed to be responsible for a limited improvement in the velocity field over and beyond the flap.

3.3 Main aerofoil at $\alpha=15^\circ$, slat at $\delta_s=15^\circ$ and flap at $\delta_f=0^\circ$

Introduction of a 15° deflected slat at $\alpha=15^\circ$, is seen to enhance the whole flow field in terms of large velocity vectors over the multi-element aerofoil and in the wake, figure 5. The elimination of the recirculating flow, evident in figure 4, and the appearance of the attached boundary layer means a great enhancement in the lift. The high velocity vectors near the leading-edge of the main aerofoil shows about 10 percent increase as compared with the case without the slat. The flap gap flow is observed to have a small effect in terms of flow field trend. On the other hand, most of the beneficial changes in the flow field is caused by the slat gap flow. In this contest it was observed that the effect of the slat wake on the boundary layer development on the main aerofoil is not very strong with only a small downstream velocity

deficit effect. The flow direction in the potential flow region experiences the least changes especially beyond the flap.

3.4 Main Aerofoil at $\alpha = 20^\circ$, slat at $\delta_s = 15^\circ$ and flap at $\delta_f = 0^\circ$

Increasing the angle of attack to 20° is seen to create larger velocities near the leading edge of the main aerofoil, figure 6, hence resulting in a higher lift. The maximum velocity for this configuration has increased to $\sim 1.55 U_\infty$ over the leading edge of the main aerofoil. However, compared to case c, $\alpha = 15^\circ$, the velocity deficit over the trailing edge of the main aerofoil and over the flap is observed to be very large, which is reflected in a wider wake. This operates against the overall enhancement of the lift.

4 Numerical Procedure

Since the experimental data, obtained using the flying hot-wire technique was not corrected for wind tunnel wall effects, the wind tunnel walls were included in the computational procedure. The wind tunnel test section extended four chord lengths upstream of the leading-edge and 4 chord lengths downstream of the trailing-edge and the computational space was divided into a number of blocks around the multi-element aerofoil using the CFX-4.2 code. The grid in the physical space was created using a body fitted coordinate system with a size of 220×100 . The flow field was obtained by solving the averaged Navier-Stokes equations using the RSM turbulence model available in the numerical code. A number of finite difference schemes are available in the code and a Curvature Compensated Convective Transport scheme (CCCT) was selected to discretise the governing equations, due to its 2nd accuracy and boundedness.

The RSM turbulence model used can not predict adequately the flowfield for all configurations. The pressure-strain, the diffusion and the dissipation terms in the exact equations for the Reynolds stress transport, contain new correlations for which model approximations must be introduced [20]. For example, for the pressure-strain which is usually

decomposed into three parts, the CFD code uses the Rotta's linear model for modelling the first part. This form does not satisfy the underlying assumption in its derivation and advanced suggestions propose a non-linear equation for it [21]. Thus, introducing the recent developments for modelling of all the correlations into the RSM turbulence model employed in commercial CFD codes probably can result in more accurate predictions.

5 Numerical predictions and comparison with experimental results

The numerical predictions of the mean velocities for the same configurations as the experimental ones are shown in figures 7 to 10 and the corresponding difference in velocity vectors, $\vec{V}_{\text{exp}} - \vec{V}_{\text{com}}$, using the experimental grids are shown in figures 11 to 14. For an angle of attack of 5° , the experimental results are shown in figure 3 the corresponding numerical predictions are plotted in figure 7. The corresponding difference plot, $\vec{V}_{\text{exp}} - \vec{V}_{\text{com}}$, shown in figure 11 demonstrates an excellent agreement over the flowfield.

The computational results for the main aerofoil at $\alpha = 15^\circ$ with the non-deflected flap, figure 8, exhibits a separated region of similar pattern to the experimental data, figure 4. Almost 50% of the main aerofoil is stalled while for the experimental results, the recirculating flow was observed to cover around 65% of the flowfield over the main aerofoil. As was explained earlier, inadequate modelling for the different correlations of the RSM turbulence model in the CFD code is partly responsible for a late start of separation [21]. The comparative velocity vector results, figure 12 demonstrates poor agreement within the separated region, and satisfactory agreement elsewhere.

Enhancement of the flow field due to employment of the advanced slat is clearly demonstrated by the computed velocity vectors depicted in figure 9. The attached flow is observed to be similar to the experimental results, figure 5, and a satisfactory agreement

exists over the whole flow field except for the shear layer near trailing edge of main aerofoil. Similar comparisons were also carried out for the three-element aerofoil for angle of attack set to 20° with a non-deflected flap. The experimental, numerical and difference results are shown in figures 6, 10 and 14 respectively. The results demonstrate that for the potential flow, the computational results are similar to the experimental results, but the numerical predictions are less accurate in the enlarged shear layer over the trailing edge of the main aerofoil and the flap.

Conclusions

The present study is mainly concerned with the effect of the advanced slat on the flow field over a multi-element aerofoil. The main method used for the present experiment is the flying hot-wire technique. The recirculating flow and unattached boundary layer which are obvious signs of the flow field deterioration over the two-element aerofoil at $\alpha = 15^\circ$ all disappeared when the advanced slat was used in front of main aerofoil. This flow field improvement is observed to extend to angles of attack as high as 20° with the non-deflected flap resulting in a higher lift.

An excellent agreement between the experimental data and the computed results was observed at an angle of attack of 5° . For other flow cases without separation (i.e. the three-element at high angles of attack of 15° and 20°), the predicted values of the mean velocity are in good agreement with the experimental data, taking into account error evaluation in both the experimental and numerical results. However, discrepancies were in particular observed in the complicated shear layers and high turbulent intensity regions due to limitations in the turbulence model and also inadequate grid resolution. When separation was present a rather high discrepancies is observed in the separated zone and a satisfactory result elsewhere.

Acknowledgements

The principle author wishes to acknowledge a study grant from government of Islamic republic of Iran.

References

- [1] Braden J A, Whipkey R R, Jones G S, and Lilley D E. Experimental study of the separating confluent boundary layer. NASA CR-3655, 1983; also AIAA paper 86-0505, 1986.
- [2] Nakayama A, Kreplin H P and Morgan H L. Experimental investigation of flowfield about a multielement airfoil. *AIAA J*, Vol. 28, No. 1, pp 14-21, 1990.
- [3] Savory E, Toy N, Tahouri, and Dalley S. Flow regimes in the cove regions between a slat and wing and between a wing and a flap of a multielement aerofoil. *Experimental Thermal and Fluid Sci.* 5, pp 307-316, 1992.
- [4] Alemdaroglu N. Experimental investigation of flow around a multielement airfoil. *AGARD-CP-515*, 1993.
- [5] Clifford-Jones J B. *An optimised slat to maximise performance in both aircraft take-off and landing.* PhD Thesis, University of Hertfordshire, UK, 1993.
- [6] Innes F, Pearcey H H and Sykes D M. Improvements in the performance of a three element high lift system by the application of airjet vortex generators. *Proc. Conf. High Lift and Separation Control*, Royal Aeronautical Society, 1995.
- [7] Moens F and Capbern P. Design and testing of leading-edge high-lift device for laminar flow wing applications. *Proc. of Conf. High Lift and Separation Control*, Royal Aeronautical Society, 1995.
- [8] Rogers S E, Wiltberger N L and Kwak D. Efficient simulation of incompressible viscous flow over single and multi-element airfoils. AIAA paper 92-0405, Jan. 1992.
- [9] Rentze K J, Buning P G and Rajagopalan R G A. comparative study of turbulence models for overset grids. AIAA paper 92-0437, Jan. 1992.
- [10] Mavriplis D J. Euler and Navier-Stokes computations for airfoil geometries using unstructured grids. *CASI Journal*, Vol. 36, No. 2, pp. 62-71, 1990.
- [11] Johnston L J. Solution of the Reynolds-averaged Navier-Stokes equations for transonic aerofoil flows. *Aeronautical Journal*, Oct. 1991, pp. 253-273.
- [12] Mavriplis D J. Multigrid solution of compressible turbulent flow on unstructured meshes using a two-equation model. AIAA paper 91-0237, Aug. 1991.
- [13] Brune G W and Sikavi D A. Experimental investigation of the confluent boundary layer of a

- multielement low speed airfoil. AIAA paper 83-0566, 1983.
- [14] Johnston L J and Horton H P. An experimental study of turbulent wake/boundary layer. *Proc ICAS-86-2.3.4*, 1986.
- [15] Mahmood Z, Khan M K, Seal WJ and Bruun H H. Comparison of measured and computed velocity fields over a high-lift aerofoil. *Proc CMEM*, 1995.
- [16] Lien F S, Chen W L and Leschziner M A. Computational modelling of high-lift aerofoils with turbulence transport models. *Proc. of Conf. High Lift and Separation Control*, Royal Aeronautical Society, 1995.
- [17] Bruun H H. *Hot-wire anemometry*. Oxford Press London, 1st edition, 1995.
- [18] Al-kayiem H H. *Separated flow on a high lift wing*. PhD Thesis, Dept. of Mech. and Manuf. Engineering, Univ. of Bradford, 1989.
- [19] Mahmood Z. *Turbulent and separated flow over multi-element aerofoils*. PhD Thesis, Dept. of Mech. and Manuf. Engineering, Univ. of Bradford, 1995.
- [20] Hinze J O. *Turbulence*. MacGraw-Hill Publishing, 1975.
- [21] Hanjalic K. Advanced turbulent closure models; a review of current status and future prospects. *Int J Heat and Fluid Flow*, Vol 15 No3, 1994.
- [22] Launder B E. Second-moment closure: present ... and future?.. *Int J Heat and Fluid Flow*, Vol. 10, No. 4, 1989.

EXPERIMENTAL INVESTIGATION OF FLOWFIELD OVER A MULTI-ELEMENT AEROFOIL AND COMPARISON WITH COMPUTATIONAL PREDICTION

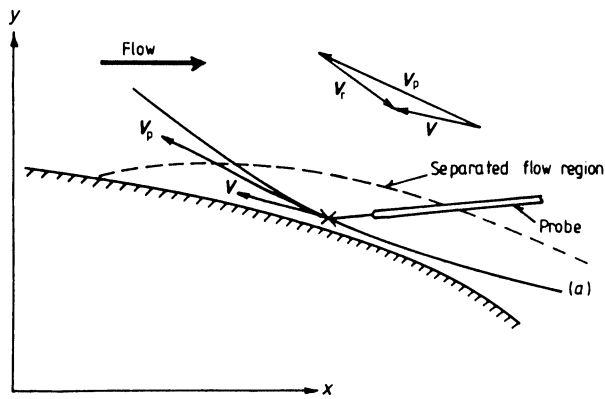


Fig 1 Measurement with flying hot-wire probe in a separated region

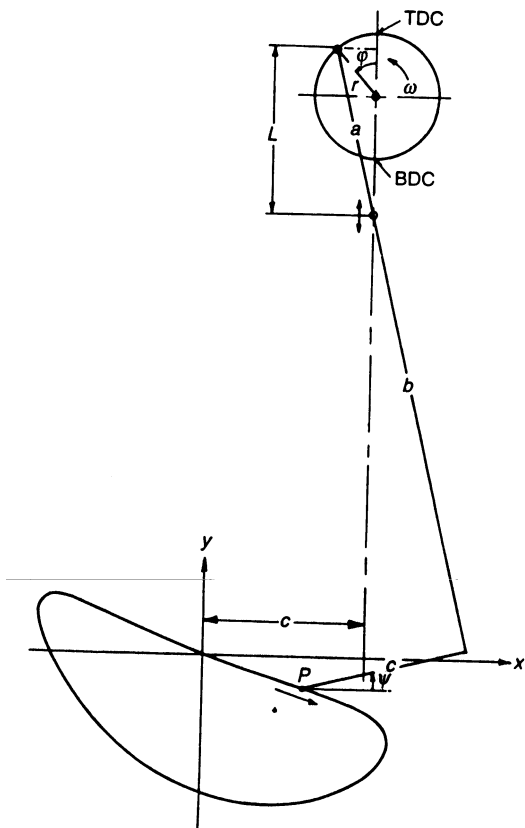


Fig 2 Four-bar flying hot-wire mechanism and notation, The geometry of that of the University of Bradford: $r = 60\text{mm}$, $a = 160\text{mm}$, $c = 146\text{mm}$, $b = 468$ and 548mm for old and new flying arm respectively

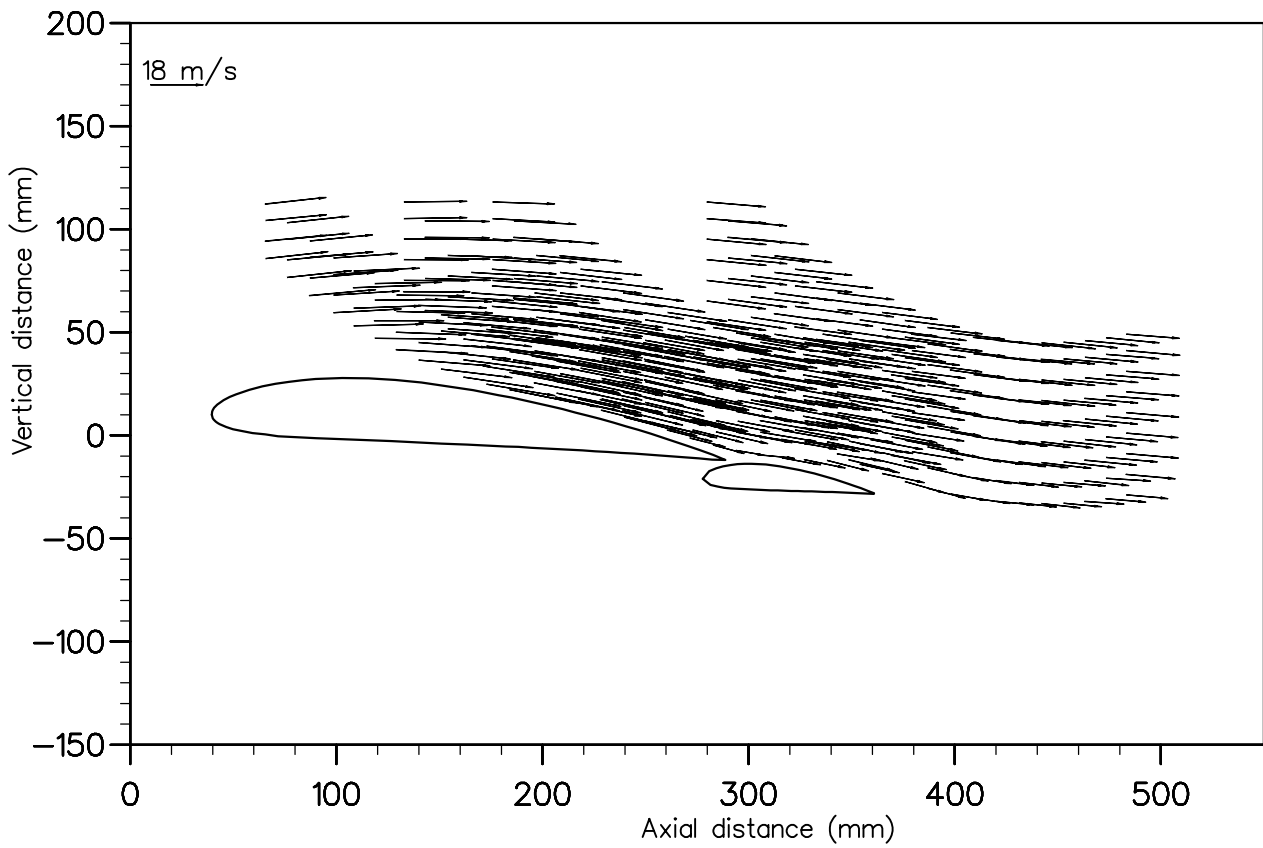


Fig 3- Mean velocity vectors for $\alpha = 5^\circ$, $\delta_f = 0^\circ$.

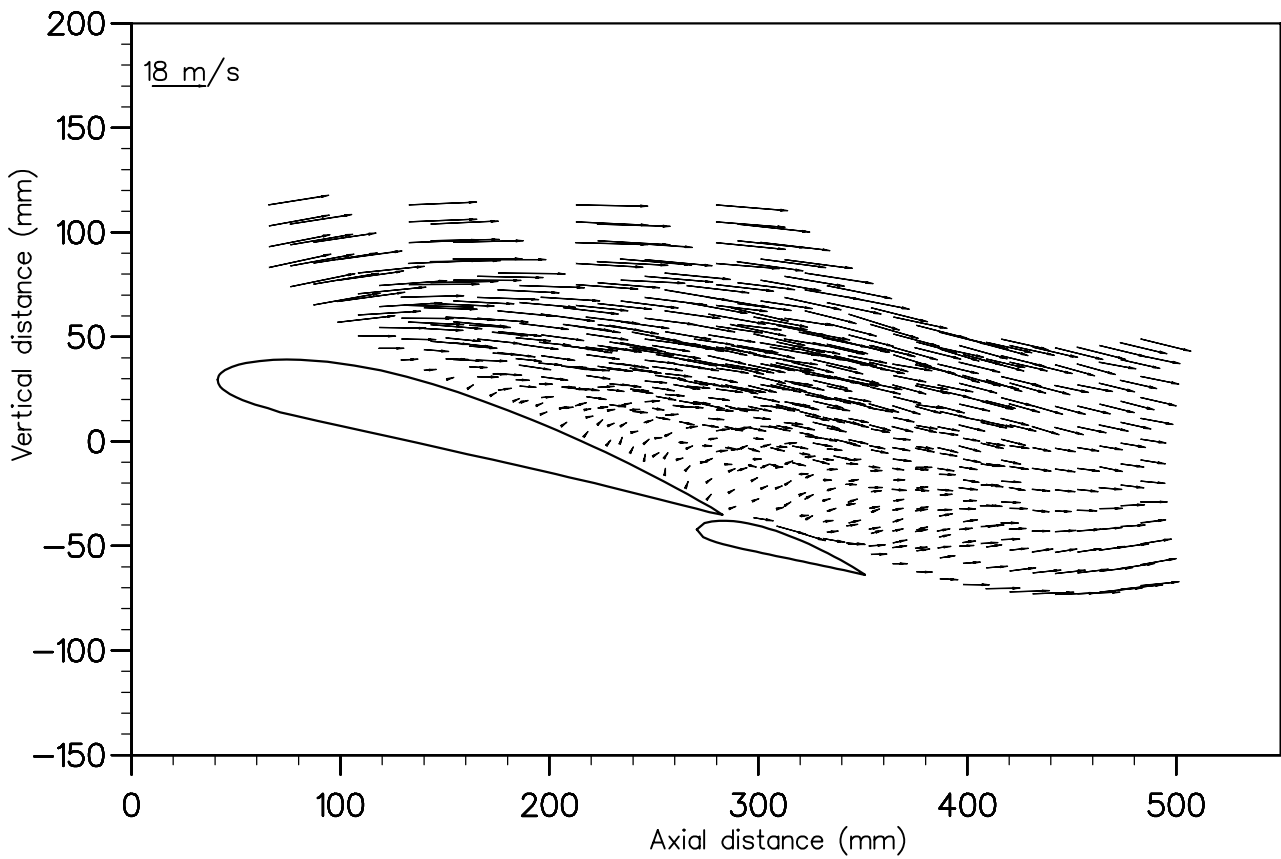


Fig 4- Mean velocity vectors for $\alpha = 15^\circ$, $\delta_f = 0^\circ$.

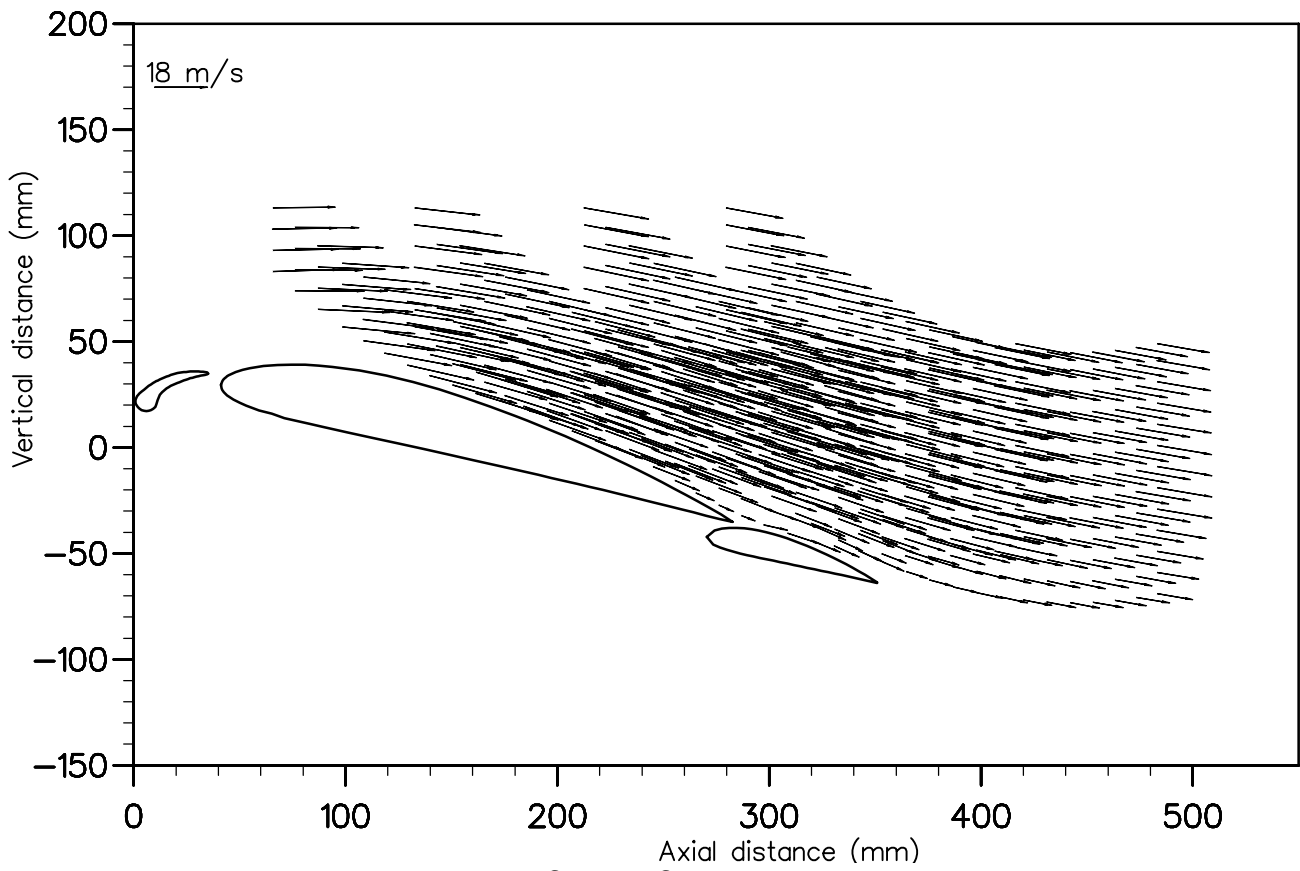


Fig 5- Mean velocity vectors for $\alpha = 15^\circ$, $\delta_s = 15^\circ$, $\delta_f = 0^\circ$.

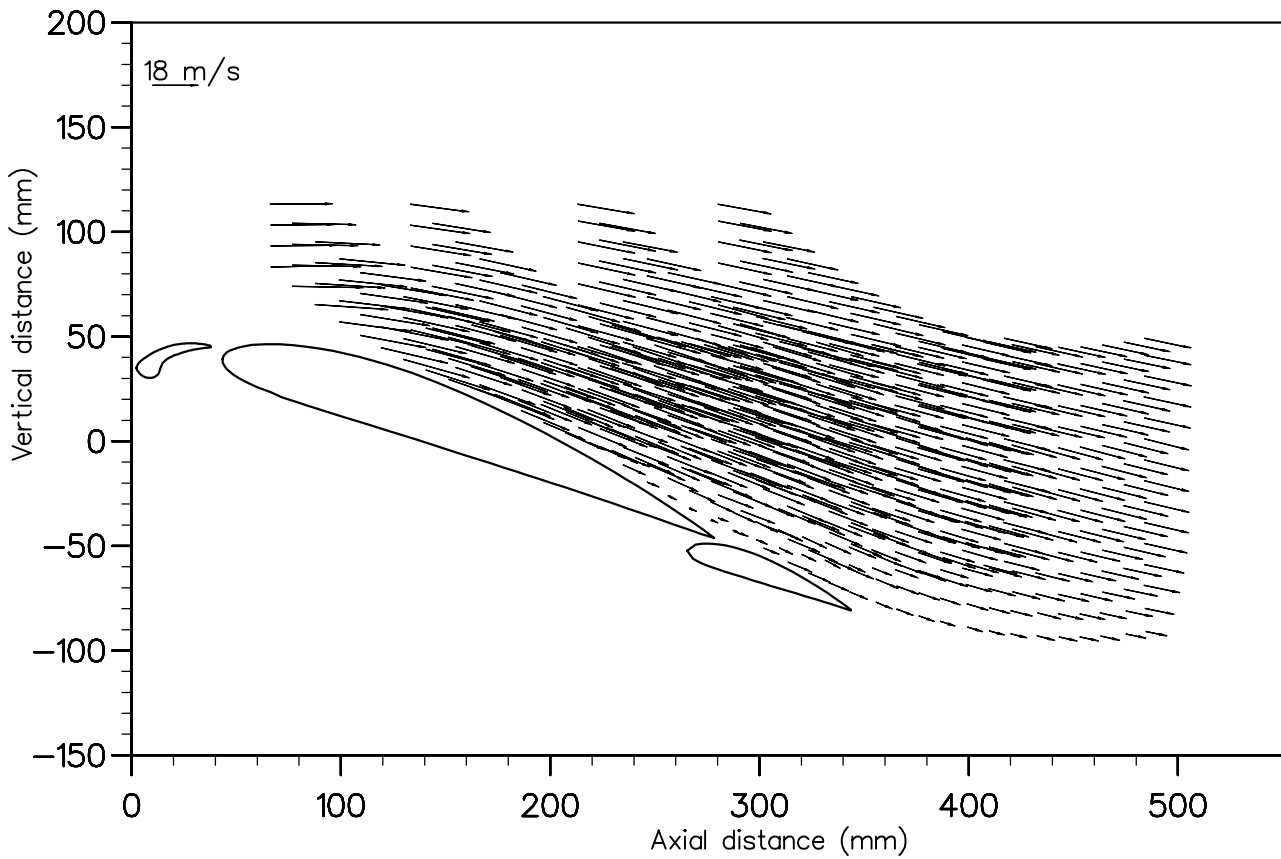


Fig 6- Mean velocity vectors for $\alpha = 20^\circ$, $\delta_s = 15^\circ$, $\delta_f = 0^\circ$.

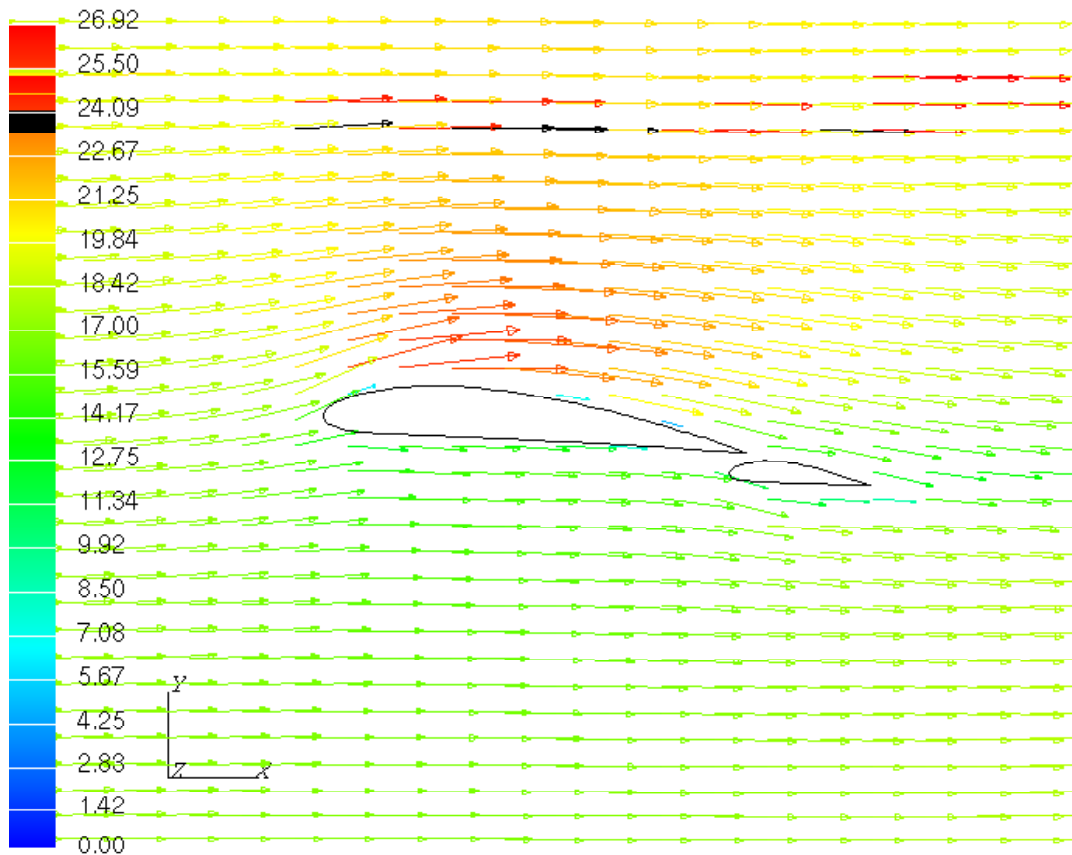


Fig 7 - Numerical prediction of mean velocity vectors for $\alpha = 5^\circ$, $\delta_f = 0^\circ$.

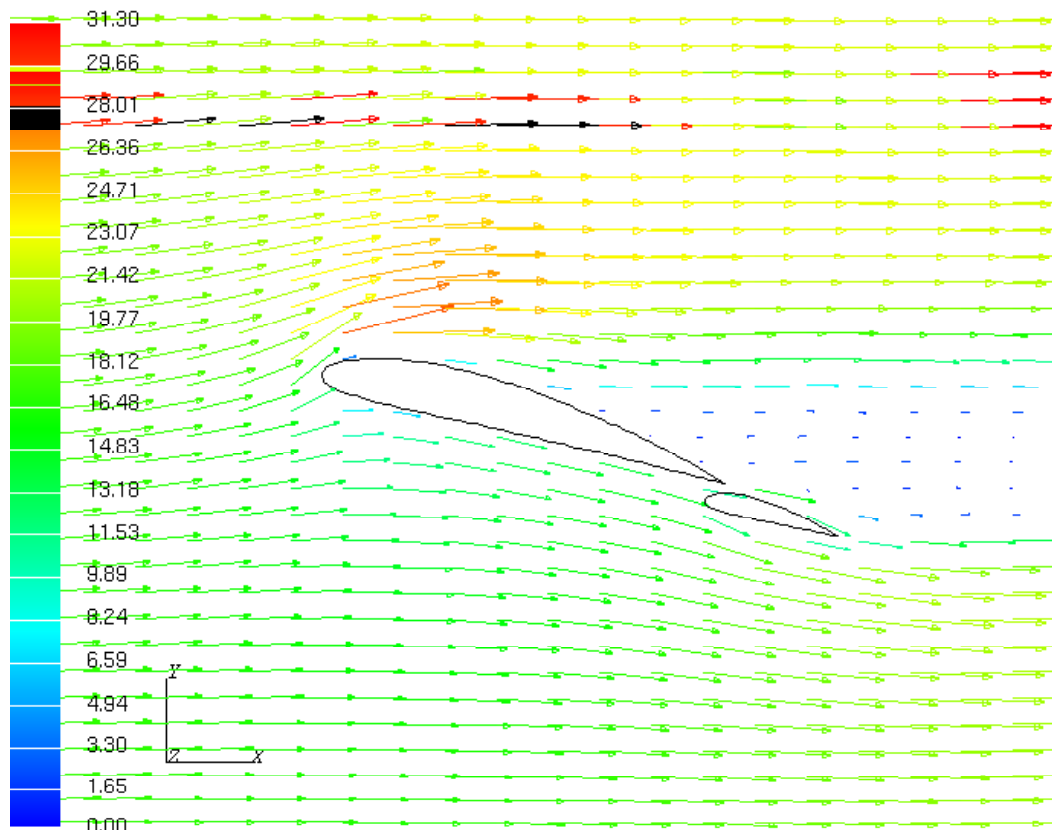


Fig 8- Numerical prediction of mean velocity vectors for $\alpha = 15^\circ$, $\delta_f = 0^\circ$.

EXPERIMENTAL INVESTIGATION OF FLOWFIELD OVER A MULTI-ELEMENT AEROFOIL AND COMPARISON WITH COMPUTATIONAL PREDICTION

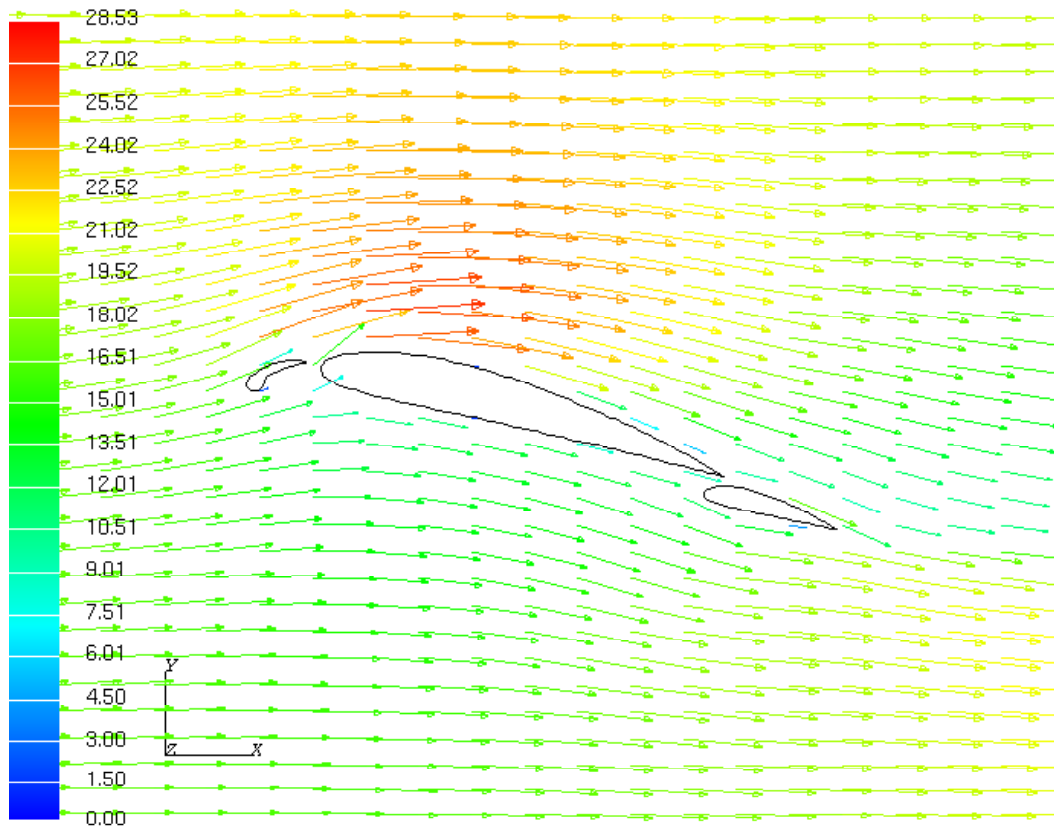


Fig 9- Numerical prediction of mean velocity vectors for $\alpha=15^\circ$, $\delta_s=15^\circ$, $\delta_f=0^\circ$.

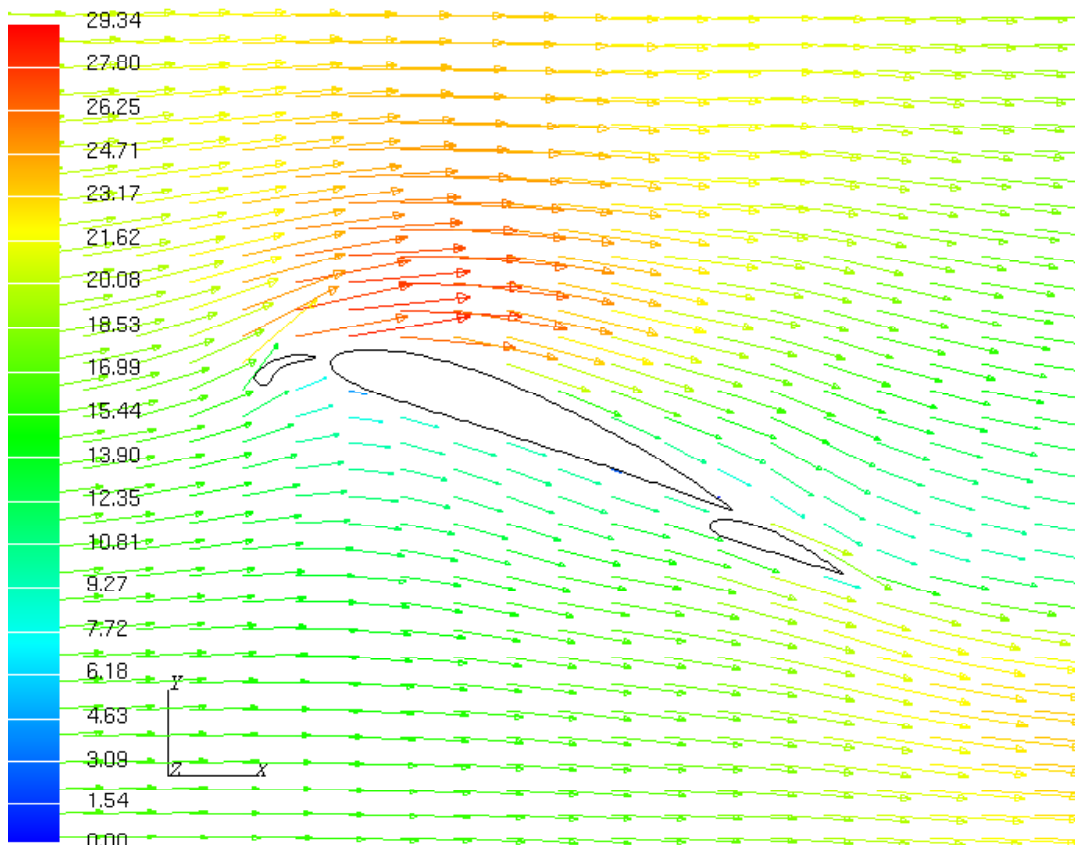


Fig 10- Numerical prediction of mean velocity vectors for $\alpha=20^\circ$, $\delta_s=15^\circ$, $\delta_f=0^\circ$.

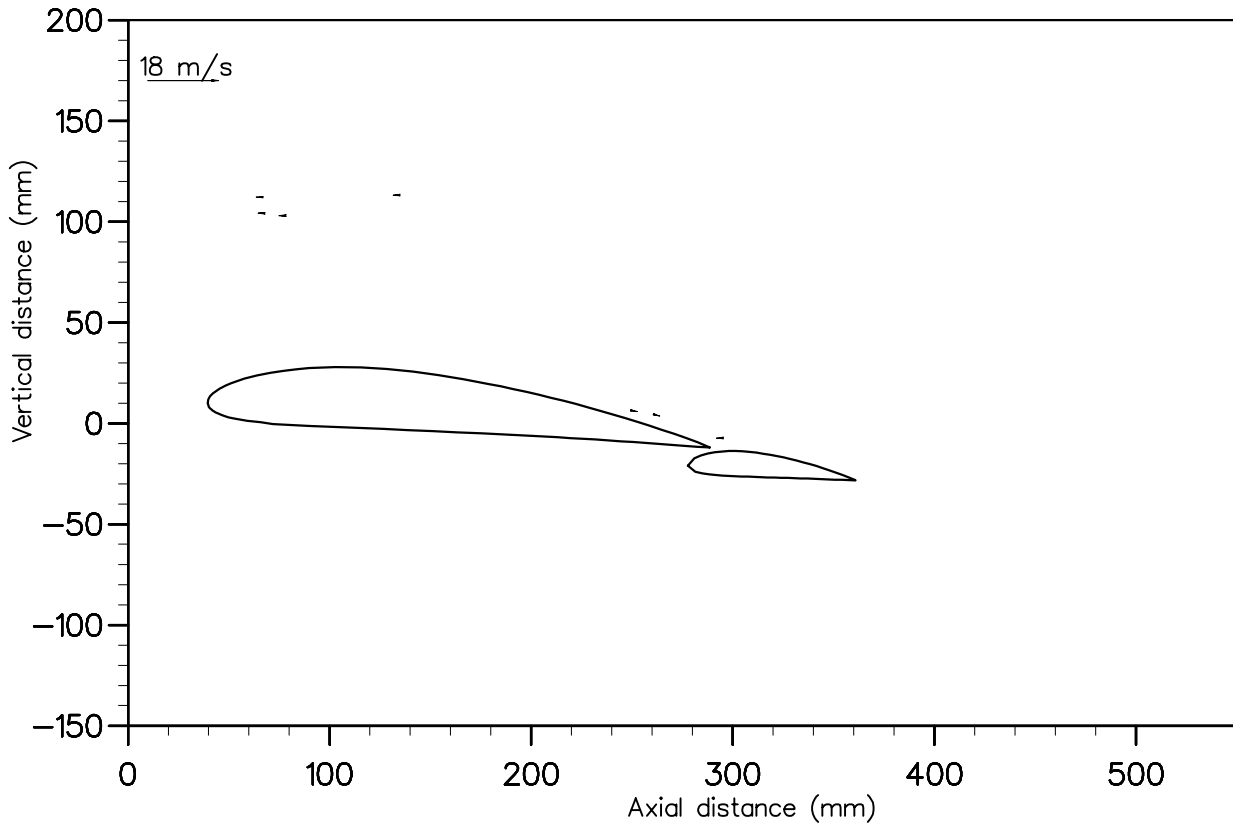


Fig 11-Mean velocity vector difference, $\vec{V}_{exp} - \vec{V}_{comp}$, for $\alpha = 5^\circ$, $\delta_f = 0^\circ$.

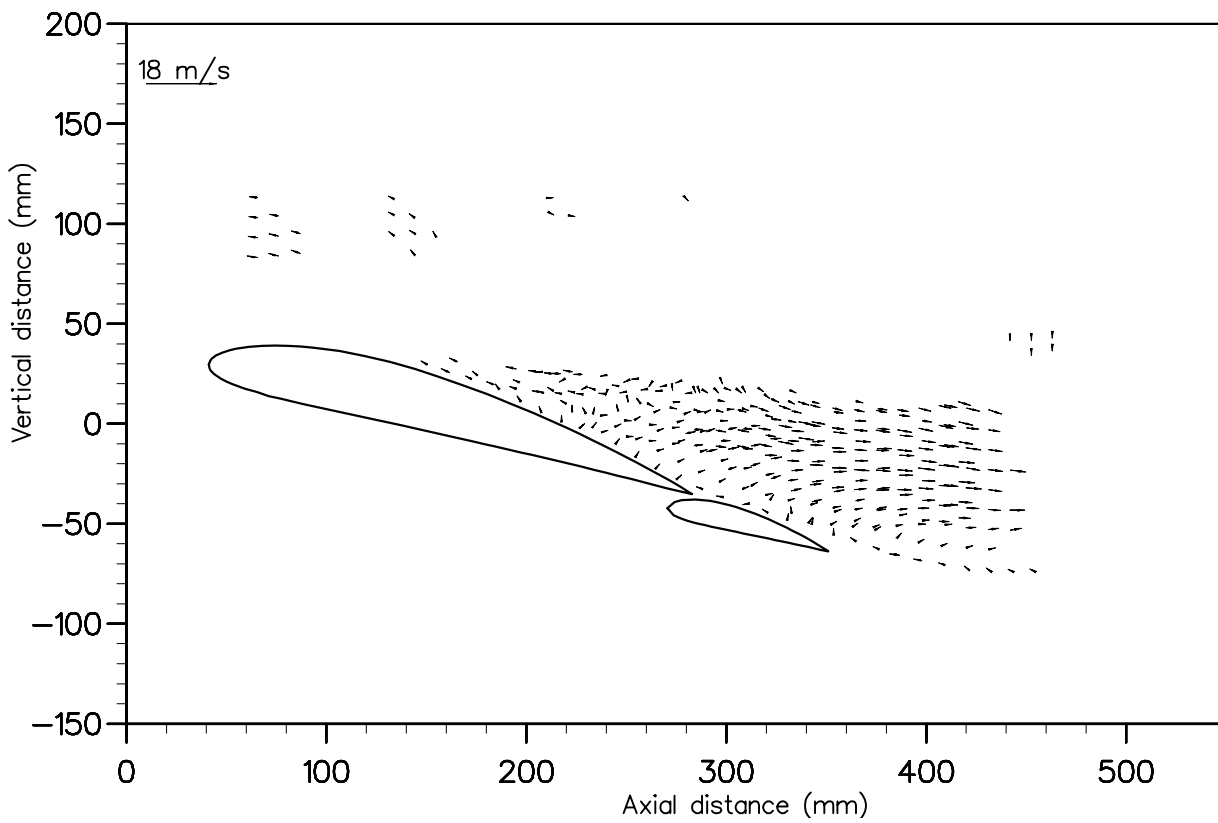


Fig 12- Mean velocity vector difference, $\vec{V}_{exp} - \vec{V}_{comp}$, for $\alpha = 15^\circ$, $\delta_f = 0^\circ$.

EXPERIMENTAL INVESTIGATION OF FLOWFIELD OVER A MULTI-ELEMENT AEROFOIL AND COMPARISON WITH COMPUTATIONAL PREDICTION

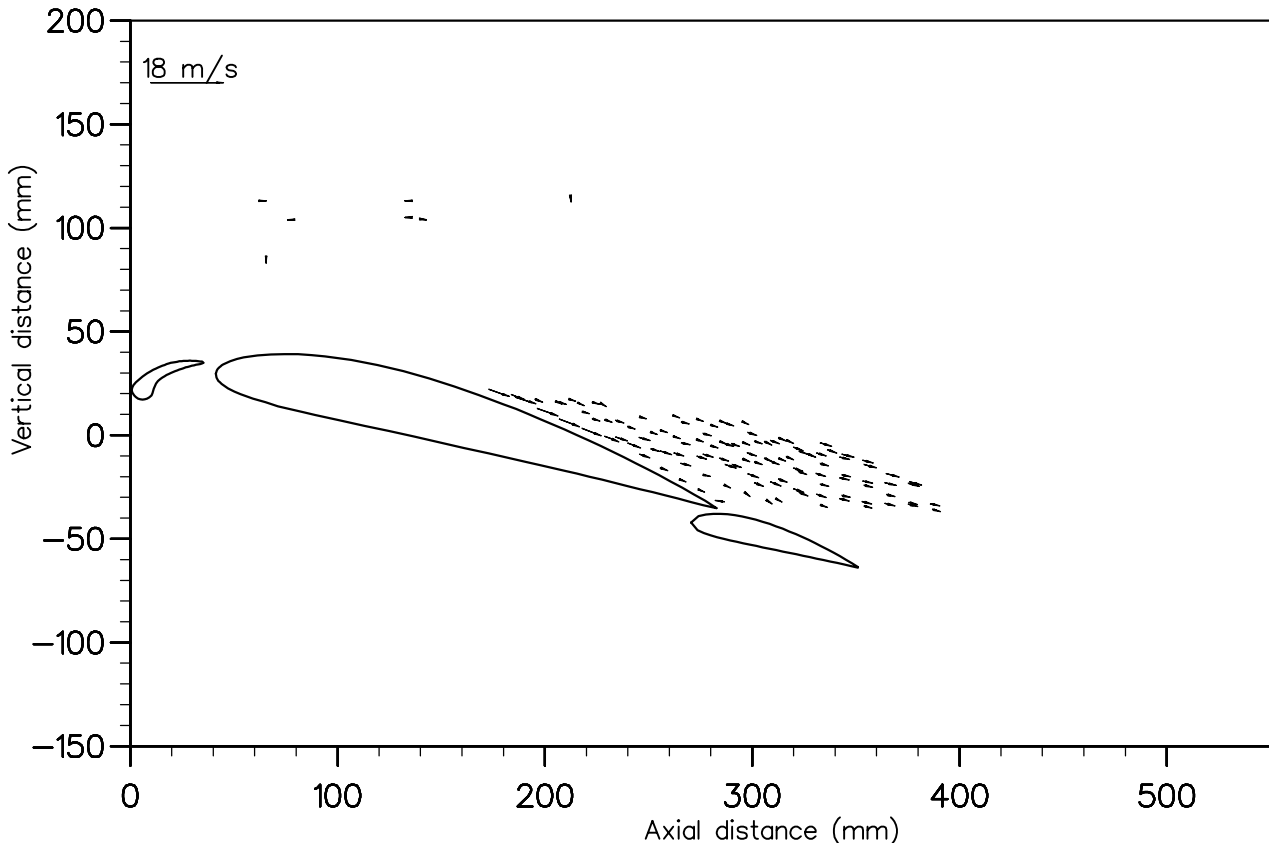


Fig 13- Mean velocity vector difference, $\vec{V}_{exp} - \vec{V}_{comp}$, for $\alpha = 15^\circ$, $\delta_s = 15^\circ$, $\delta_f = 0^\circ$.

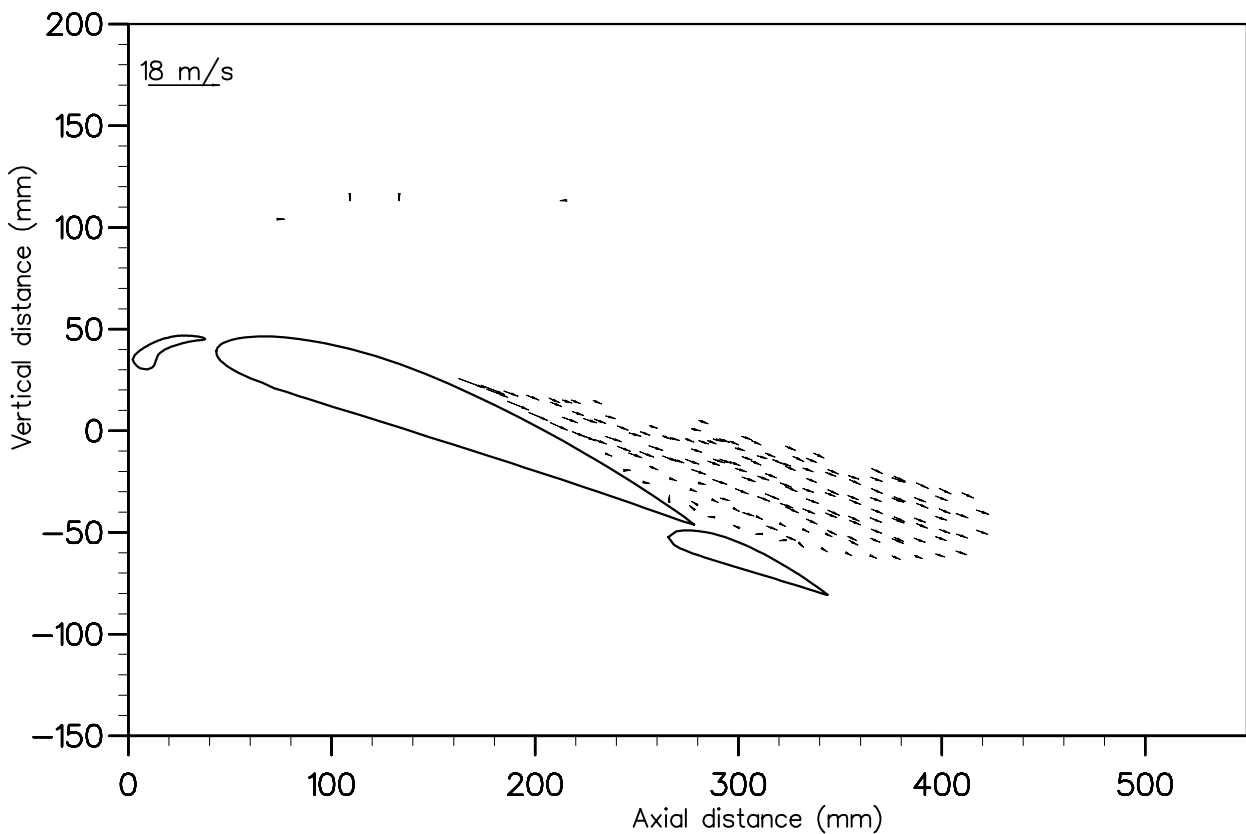


Fig 14- Mean velocity vector difference, $\vec{V}_{exp} - \vec{V}_{comp}$, for $\alpha = 20^\circ$, $\delta_s = 15^\circ$, $\delta_f = 0^\circ$.